Experimental and theoretical investigation of Li-ion battery active materials properties: Application to a graphite/Ni0.6Mn0.2Co0.2O2 system

Oumaima Chaouachi, Jean-Michel Réty, Sylvie Génies, Marion Chandesris, Yann Bultel

Experimental and theoretical investigation of Li-ion battery active materials properties: application to a graphite/ $Ni_{0.6}Mn_{0.2}Co_{0.2}O_2$ system

Oumaima Chaouachi[a,b], Jean-Michel Réty[a], Sylvie Génies[b], Marion Chandesris[b*],Yann Bultel[c]

[a]*Forsee Power, 1 Boulevard Hippolyte Marquès, 75013 Paris, France*

[b]*Univ Grenoble Alpes, CEA LITEN 17 Rue des Martyrs, F-38054 Grenoble Cedex 9, France*

[c]*Univ. Grenoble Alpes, Univ. Savoie Mont Blanc, CNRS, Grenoble INP, LEPMI, 38000 Grenoble, France*

*marion.chandesris@cea.fr

Keywords: Li-ion batteries, electrochemical impedance spectroscopy, Modeling, active material properties, Reference electrode

Abstract:

The knowledge of active materials properties and their evolution with aging is crucial to simulate and predict with a high reliability the electrochemical performance of lithium-ion batteries. In view of developing more accurate physics-based Lithium Ion Battery (LIB) models, this paper aims to present a consistent framework, including both experiments and theory, in order to retrieve the active material properties of commonly used electrodes made of graphite at the negative and $Ni_{0.6}Mn_{0.2}Co_{0.2}O_2$ (NMC 622) at the positive, as function of the active materials stoichiometry. To measure the equilibrium potential and the solid diffusion coefficient, Galvanostatic Intermittent Titration Technique (GITT) measurements were used. Electrochemical impedance spectroscopy (EIS) measurements with reference electrodes were performed to determine the exchange current density using the transmission line model. The measured stoichiometry dependence of these three active material properties has been further analyzed, based on thermodynamic considerations. For the positive material, a model is proposed highlighting the non-ideal behavior of lithium inside the host material. The thermodynamic relations available in the literature are not directly transposable to the $Ni_{0.6}Mn_{0.2}Co_{0.2}O_2$ material, suggesting the necessity to account for supplementary terms. Nevertheless, the proposed stoichiometry dependent laws determined with the same stoichiometry definition go already beyond most reported values for the $Ni_{0.6}Mn_{0.2}Co_{0.2}O_2$ and can be used to increase the predictability of multi-physics lithium-ion battery models.

1. Introduction

Lithium ion batteries (LIB) have been considered as a technological and commercial success since their first commercialization by SONY in 1991. Due to their advantageous characteristics such as their high energy density and power capabilities, this technology is equipping a growing number of applications ranging from small-scale electronic gadgets to automotive vehicles [1]. Optimization of LIB performances for various usages requires the understanding and the knowledge of the different physical mechanisms of the battery with a sound quantification. Mathematical models are a useful tool to decouple and to quantify these different mechanisms, and to understand their evolution along the lifetime of the battery. A huge research effort devoted to battery modeling started in the 60s with different approaches such as Equivalent Electric Circuit (EEC) models [2], but also electrochemical ones like the so called porous electrode model introduced by Newman and Tiedeman in 1975 [3, 4] and applied on LIB in the 90s [5]. On one hand, EEC models, considered as semi-empirical models, simplify the multi-physics behavior of the cell to obtain a representation with an electric circuit, which makes them easy to implement in a Battery Management System (BMS). On the other hand, electrochemical models, based on the computation of physical phenomena at the electrode scale, allow predicting the electrochemical behavior of the system, for various operating conditions and/or electrodes designs, which make them a powerful tool for optimization. These models however require an accurate description and a coupling of the different physics, to account for electrochemical reactions, mass and charge transports as well as thermal effects. In particular, the knowledge of the physical properties of the different components of the LIB is key in this approach to ensure a high level of predictability. Among these physical properties, it is crucial to determine accurately those related to the active materials, such as the equilibrium potential, the lithium solid diffusion or the exchange current density as these properties are affecting significantly the models results.

Up to day, many studies have been carried out to understand the physical and electrochemical mechanisms that take place in the different cell components, to determine the most important physical parameters and how they can be implemented in models. In the literature, many experimental protocols are proposed to measure geometric and physical parameters of the electrodes such as electronic conductivity, porosity, active material equilibrium potential or lithium diffusion coefficient [6]. Electrochemical Impedance Spectroscopy (EIS) has been considered as a standard method to estimate fundamental physical properties, to investigate

reaction mechanisms and to characterize batteries [1], [7], [8], [9]. It is an effective tool to follow concurrently the resistive, capacitive and the inductive behaviors of the system. The exploitation of the EIS results can help to figure out many physical phenomena such as solid phase diffusion, charge transfer kinetics and ion transport by using their frequency dependent characteristics. Moreover, in the literature, EIS measurements have been used to study electrode/electrolyte interface [10], electrolyte performance [11], and to evaluate the aging by following the SEI resistance [12], [13]. It has been also used to study the kinetics of charge transfer in Li-ion batteries and evaluate precisely the exchange current density i_0. Generally, a simple R-C element model is implemented to extract i_0 from an impedance spectrum [14]. However, this model assumes a semi-circle shape for the charge transfer resistance in the impedance spectra which is not always observed in the experiments with porous electrodes. Transmission line model (TLM) [15], [16] is more appropriate to take into account the non-semicircle shape of the impedance spectra in the middle to high frequency range that porous electrode may cause. Another central electrochemical technique to determine active material properties is the Galvanostatic Intermittent Titration Technique (GITT). Since the pioneering work of Weppner and Huggins [17], it has been used with a growing interest to retrieve the equilibrium potential and transport parameters of various active materials [17], [18], [19], [6].

Regarding active material properties, equilibrium potential curves with a dependence on the stoichiometry are most of the time implemented in multi-physics models, as this dependence is well recognized. Furthermore, to simplify their implementation in the different models, analytic expressions are sometimes suggested as the one proposed by Doyles (1995) [20] to model the equilibrium potential of the active material as function of the state of charge (SOC). However, this stoichiometry dependence is rarely transposed to the other active material properties. Indeed, many models use constant values for the solid diffusion D_s while the exchange current density i_0, is modeled with a stoichiometry dependence of the form $y^{\alpha}(1-y)^{1-\alpha}$ arising from the classical Butler-Volmer relation [21], [22]. Such an approach does not take into consideration the non-ideal interactions between ions in intercalation materials and does not take into account the interdependence between the active material properties. A more thermodynamically consistent approach has been proposed by Bazant studying the electrochemical kinetic of Li insertion in lithium iron phosphate ($LiFePO_4$) active materials [23]. This approach highlights the links between the active material properties toward the stoichiometry dependence and provides expressions that can be implemented in LIB models. If this thermodynamic approach exists for $LiFePO_4$ active materials, it is

however missing for other active materials currently used in commercial cells, such as graphite or transition metal oxides of the Ni-Mn-Co family.

In view of developing more accurate physics-based LIB models, this paper aims to present a consistent framework, including both experiments and theory, in order to retrieve the active material properties of commonly used electrodes made of graphite at the negative and $Ni_{0.6}Mn_{0.2}Co_{0.2}O_2$ at the positive, as function of the active materials stoichiometry. To measure the equilibrium potential and the solid diffusion coefficient, GITT measurements were used, while EIS measurements with reference electrodes were performed to determine the exchange current density and were analyzed using a TLM model [15], [16]. Then, the measured stoichiometry dependence of these three active material parameters is further analyzed, based on thermodynamic considerations. For the $Ni_{0.6}Mn_{0.2}Co_{0.2}O_2$ active material, a model is proposed to account for this observed stoichiometry dependence, highlighting the non-ideal molecular behavior of lithium inside the host material.

2. Experimental

2.1 Materials:

A NMC-based positive electrode (PE) was prepared by coating a dispersion of a polycristalline Li-$Ni_{0.6}Mn_{0.2}Co_{0.2}O_2$ (Umicore), Super P65 (Imerys) with an exchange surface area of 65m²/g and VGCF-H from Showa Denko as carbon conductive additive and PolyVinyliDene Fluoride (PVDF) as a binder with 92:2:2:4 weight ratio, on an aluminum foil. The graphite-based negative electrode (NE) was prepared similarly, by using a mixture of spherical graphite with CMC (Ashland) and SBR (BASF) binders (sodium carboxymethyl cellulose and styrene butadiene rubber) with 97.4:1.3:1.3 weight ratio, coated on a copper foil. The average particles sizes $\boldsymbol{r_{50}}$ have been measured by laser granulometry and are around 6.6µm for the $Ni_{0.6}Mn_{0.2}Co_{0.2}O_2$ and 7.88µm for the graphite.

The two electrodes were prepared using a laboratory in house process [24]. The components were mixed using a planetary mixer, using deionized water as solvent for the negative electrode and NMP solvent for the positive electrode. The slurry was then coated onto the current collectors. A custom reverse roll coater installed in dry room with 1.5 m drying oven was used for both electrodes which were then calendared to reach the desired porosity. They were manufactured considering a loading of 18.2 mg/cm² for the positive and 10.8 mg/cm² for the graphite with a porosity of 24% and 26% respectively. With the estimated reversible capacity, these loadings correspond to 3.43 mAh/cm² and 3.78 mAh/cm², which leads to a

face to face N/P ratio of 1.1. The separator is a 25 µm thick mono-layer (PP) Celgard 2400. The electrolyte (UBE) consists of 1M of lithium hexafluorophosphate (LiPF6) in 1:1:1 weight proportion of ethylene carbonate (EC), ethyl methyl carbonate (EMC), and dimethyl carbonate (DMC), whose purity limit is 5 ppm of H2O, 10 ppm of HF. For the different designs, the electrolyte is put in large excess to get a full wetting of the electrodes and avoid electrolyte starvation.

2.2 Designs:

The first design is a so-called half-cell design in coin cell (CC) format. It is a CR2032 coin cell format made of stainless steel and it consists of a top cover, bottom container spacer and spring. This design consists of the tested active materials electrode as working electrode (graphite in case of the NE and $Ni_{0.6}Mn_{0.2}Co_{0.2}O_2$ in case of the PE) with a 14mm diameter and a lithium foil as counter electrode, with a 16mm diameter. The exchange surface areas $\boldsymbol{S_{AM}}$ for this coin cell design are estimated from the knowledge of $\boldsymbol{r_{50}}$ and assuming that particles are spherical, giving a value around 3.31m² for the $Ni_{0.6}Mn_{0.2}Co_{0.2}O_2$ and 2.68m² for the graphite (Summary in table 1). This coin cell design will be used to perform GITT measurements in order to extract equilibrium potentials and diffusion coefficients of both active materials.

The second design is a pouch cell containing the two tested electrodes (graphite for the NE, $Ni_{0.6}Mn_{0.2}Co_{0.2}O_2$ for the PE) with a lithium foil reference electrode inserted between the PE and the separator an covered with an extra separator to avoid short circuit, as described Fig. 1a. An aluminum tab is ultrasonically welded to the positive electrode, while a nickel one is welded to the negative. The pouch cells are assembled in a dry room (-20°C dew point) and filled with electrolyte in an Argon filled glove box. The pouches are put under partial vacuum and the all sandwich is sealed using a heatsealer. The electrode surface areas $\boldsymbol{S_g}$ are for the positive electrode 10.24 cm² (3.2x3.2) and for the negative 12.25 cm² (3.5x3.5). These dimensions are chosen to ensure a good coverage of the positive electrode by the negative one, while trying to keep this mismatch as low as possible. Indeed, this mismatch implies an increase of the irreversible capacity with lithium consumed at the negative electrode during its first lithiation due to SEI formation. This area mismatch leads to a lower utilization of the cathode with, at the cell scale, an electrode capacity ratio N/P of 1.3 instead of the "face to face" N/P ratio of 1.1. The exchange surface areas $\boldsymbol{S_{AM}}$ for this pouch cell design are

estimated from the knowledge of r_{50} giving a value around 22.03m² for the $Ni_{0.6}Mn_{0.2}Co_{0.2}O_2$ and 22.28m² for the graphite (Summary in table 1).

For EIS measurements, the choice of the reference electrode is a key issue. In the literature, lithium foil is often used as a reference electrode for electrochemical characterization in the conventional 3-electrode design (Fig. 1a) [25]. However, this kind of reference electrode suffers from a low stability [26] and can also cause artificial EIS response detected in Nyquist plots as a "spiral" type behavior, leading to a lack of reproducibility [27]. These effects make them non-efficient for investigations during aging or involving impedance measurements. Alternative solutions are proposed in the literature to limit these effects. As reference electrodes must have a stable potential over a large SOC range, lithium titanate ($Li_4Ti_5O_{12}$) and $LiFePO_4$ have recently attracted considerable attentions as reference electrodes for EIS [28], [29], [30], [31], [32], [33]. For the present work, $LiFePO_4$ is used as a reference electrode. The electrode is prepared by mixing a commercial $LiFePO_4$ active material from BeLife with Super P65 as carbon conductive additive and PVDF as binder before a coating on an aluminum mesh. This reference electrode is inserted inside the 4-electrode pouch cell design presented Fig. 1b. The Li reference electrode is kept in the system to control the potential of the electrodes. A partial delithiation of $LiFePO_4$ is performed *in situ* once the cell is assembled and charged at a C/50 rate to reach the 3.48V *vs* Li^+/Li potential plateau and a stoichiometry of 0.5.

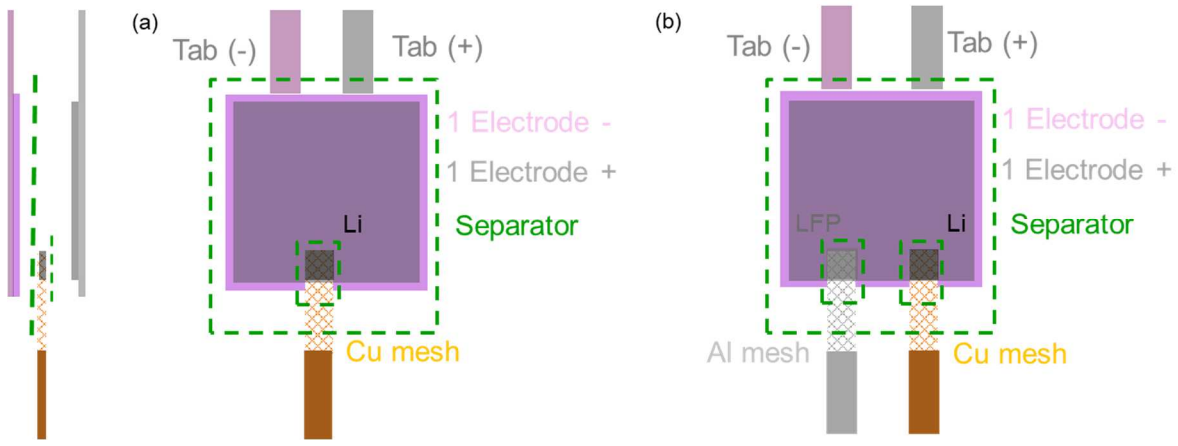

Fig. 1: Schematic description of (a) the 3-electrodes pouch cell design with (left) side view and (right) top view and (b) the 4- electrodes pouch cell design from top view.

The pouch cell design with one reference electrode has been used to perform a GITT measurement. The aim is to retrieve a relation between the SOC of the pouch cell design and the stoichiometries of the two active materials. The second design with two reference electrodes has been used to perform EIS at different SOC and deduce the exchange current densities of the active materials as function of their stoichiometry.

2.3 Electrochemical measurements:

After assembly, pouchs are put in a mechanical homemade design, where a homogeneous force of roughly 100N is applied, which corresponds to a pressure of 1bar on the 10 cm^2 surface. A formation protocol at 25°C is applied to the coin and the pouch cells. For $Ni_{0.6}Mn_{0.2}Co_{0.2}O_2$ vs. Li coin cells, it consists of two full charge/discharge cycles between 2.6 and 4.3V at C/20. For graphite vs. Li coin cells and the pouch cell designs, it consists of one cycle at C/20 followed by 3 cycles at C/5 of full discharge/charge applied between 10mV and 1V and 2.5 and 4.2V respectively. This last protocol is performed to ensure the formation of a stable Solid Electrolyte Interphase (SEI) on the graphite particles. The C-rate for the formation cycles is estimated from the reversible capacity of the electrodes measured in dedicated experiments. For the subsequent C-rates, the capacity measured during the formation at C/20 is used to recompute the C-rate. All the electrochemical measurements on coin cells or pouch cells were performed using a modular potentiostat/galvanostat/EIS VMP3 from Bio-Logic, Seyssinet-Pariset, France.

GITT protocol: GITT experiment consists of series of current pulses at a fixed value followed by rest periods. This sequence is repeated until the battery is fully charged and discharged. This protocol is used to determine the equilibrium potential and lithium diffusion coefficient of active materials [17], [18], [19]. In this study, a series of pulses is applied to the cell at a fixed current of C/10 during 12 minutes, followed by a 4h relaxation time. The sequence is repeated 50 times until complete charge or discharge of the cell. GITT tests were performed on $Ni_{0.6}Mn_{0.2}Co_{0.2}O_2$ *vs.* Li and graphite *vs.* Li coin cells, as well as in the pouch cell design with a Li reference electrode. During the pulse period, data are recorded at every voltage increment/decrement of 1mV. The GITT protocol is applied after formation of the cells and is performed in both charge and discharge. It is started in charge for $Ni_{0.6}Mn_{0.2}Co_{0.2}O_2$ vs. Li and full cell configurations, and in discharge for graphite vs. Li.

Electrochemical Impedance Spectroscopy (EIS) protocol: During an EIS measurement, alternative sinusoidal potential excitations are applied to the electrochemical cell at various frequencies, while measuring the resulting currents. These current signals are analyzed at the different frequencies to obtain the cell impedance spectra. This measurement is performed by using an excitation signal with a small amplitude to obtain the pseudo-linear response of the cell. In this study, Potentio-Electrochemical Impedance Spectroscopy (PEIS) measurements were performed at different SOC on the pouch cell with $LiFePO_4$ reference electrode. The measurements were done in potentiostatic mode with a voltage amplitude of 5mV. The frequency range was set to 200 kHz-0.1 mHz with 8 points per decade. Impedance spectra were measured at room temperature. To reach the desired SOC, a galvanostatic discharge at C/10 is applied during 1h, followed by a rest period of 1h to reach equilibrium before the PEIS measurement. This protocol is repeated 10 times to complete the lithiation process. It is applied in discharge after the cell formation protocol and a first charge of the cell until the cut off voltage of 4.2V.

3. Experimental results

In this section, we present the active material properties obtained from the electrochemical measurements. During the results analysis, special attention has been put on the stoichiometry determination to latter allow material properties comparison.

3.1 Equilibrium potential

Equilibrium potential, E_q of an active material inside an electrode is reached when the chemical potentials of lithium in both phases, *i.e.* at the interface between the active material and the electrolyte, are equal. Using GITT methods, E_q is identified at the end of each relaxation period [34]. For the coin cell designs, *i.e.* working electrode vs. Li, the measured open circuit potential (OCP) corresponds to the equilibrium potential of the studied material. The results obtained for $Ni_{0.6}Mn_{0.2}Co_{0.2}O_2$ and graphite in both lithiation and delithiation are shown Fig. 2 as function of the material stoichiometry, together with the averaged value.

For the graphite (Fig. 2a), the stoichiometry range is defined by assuming that, at the end of the first lithiation the material stoichiometry, $y_{max}^{CC,Gr}$ is equal to one, and by using the subsequent delithiation to determine the reversible capacity $Q_{rev}^{CC,Gr}$, which is reached in our case at 356 mAh/g with a first irreversible capacity ($Q_{irrev}^{CC,Gr}$) of 28 mAh/g. This value is slightly lower than the theoretical capacity Q_{th}^{Gr} equals to 372 mAh/g. This theoretical capacity

is used to calculate the minimum stoichiometry ($y_{min}^{CC,Gr}$) corresponding to the delithiated graphite, with the following equation, and we obtain a value of 0.045:

$$y_{min}^{CC,Gr} = \frac{Q_{th}^{Gr} - Q_{rev}^{CC,Gr}}{Q_{th}^{Gr}} \quad (1)$$

For the graphite (Fig. 2a), the three classical potential plateaus are observed with a slope close to zero and two transitions regions for stoichiometry around 0.17 and 0.5. A slight difference between the lithiation and delithiation curves is observed, but only during these transition regions. The potential plateaus correspond to coexistence of two-phases in the solid material, while only one phase exists in the transition regions [35]. The derivative of the equilibrium potential versus stoichiometry, obtained from the average value, is also presented and highlights the variation of the potential during the transition regions.

For the $Ni_{0.6}Mn_{0.2}Co_{0.2}O_2$, the stoichiometry range is calculated considering the theoretical value (Q_{th}^{NMC}) of 276.7 mAh/g and by assuming that the material is fully lithiated before formation. The measured reversible capacity ($Q_{rev}^{CC,NMC}$) of 184 mAh/g is determined from the lithiation step, by taking into account the first irreversible capacity ($Q_{irrev}^{CC,NMC}$) of 21 mAh/g. The maximum and minimum stoichiometries of $Ni_{0.6}Mn_{0.2}Co_{0.2}O_2$ in lithiation $y_{max}^{CC,NMC}$ and delithiation $y_{min}^{CC,NMC}$ are respectively given by:

$$y_{max}^{CC,NMC} = \frac{Q_{th}^{NMC} - Q_{irrev}^{CC,NMC}}{Q_{th}^{NMC}} \quad (2)$$

$$y_{min}^{CC,NMC} = \frac{Q_{th}^{NMC} - (Q_{rev}^{CC,NMC} + Q_{irrev}^{CC,NMC})}{Q_{th}^{NMC}} \quad (3)$$

Leading to a variation range of [0.259 – 0.92]

As presented in (Fig. 2b), there is almost no difference between lithiation and delithiation measurements, which confirm that the equilibrium state is reached at the end of the relaxation periods. The equilibrium potential for $Ni_{0.6}Mn_{0.2}Co_{0.2}O_2$ steadily decreases when the

stoichiometry increases with a higher slope at low stoichiometry. It is highlighted on the derivative of the average equilibrium potential that the slope is almost constant for a stoichiometry above 0.65.

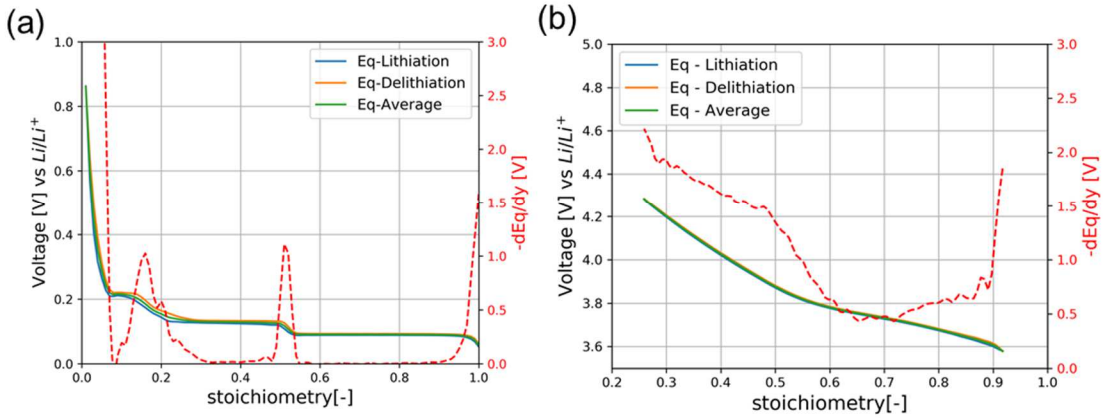

Fig. 2: Equilibrium potentials measured in half-cell configuration in lithiation and delithiation together with the average value and its derivative versus stoichiometry (a) Graphite vs Li (b) $Ni_{0.6}Mn_{0.2}Co_{0.2}O_2$ vs Li

For electrochemical experiments in full cell configuration, material properties are measured as function of the SOC of the cell. To get the active material properties as function of their own stoichiometry, a relation between the active materials stoichiometry and the SOC of the cell is required. In this work, we have used the GITT experiment in pouch cell format with a reference electrode to obtain these relations. Indeed, the lithium reference electrode gives access to the positive and negative equilibrium potentials within the full cell and allows following the stoichiometry variation range of both electrodes along the equilibrium curves.

Fig. 3a shows the cell OCP together with the electrode potentials extracted from the GITT experiment in the pouch cell format as function of the cell capacity. Computed OCP results of $Ni_{0.6}Mn_{0.2}Co_{0.2}O_2$ and graphite from the CC results are also presented as function of the pouch cell capacity Fig. 3a. To perform this comparison, the capacities of $Ni_{0.6}Mn_{0.2}Co_{0.2}O_2$ and graphite measured per masse of active material in the CC design, are multiplied by the masses of active material used in the pouch format. Furthermore, the computed CC results are then shifted so as to be superposed with the pouch cell results. A very good superposition is obtained. These operations allow to have a first overview of the stoichiometry ranges used for the two electrodes. We can notice that with the present design, only 56% of the negative electrode capacity is used. Indeed, as shown in Fig. 3a, the two upper plateaus of the graphite are used with the pouch format, and only a small portion of the lower one.

The maximum stoichiometry in the pouch design is calculated considering the theoretical capacity and the irreversible capacity of the pouch formation as:

$$y_{max}^{Pouch,NMC} = \frac{Q_{th}^{NMC} - Q_{irrev}^{pouchNMC}}{Q_{th}^{NMC}} \quad (4)$$

Since, the irreversible capacity $Q_{irrev}^{pouch,NMC}$ expressed as function of positive active material is higher in the pouch cell format due to SEI formation on the negative electrode and area mismatch, $Q_{irrev}^{pouch,NMC} = 42$ mAh/g, it leads to a maximum stoichiometry of 0.848, which is lower than in the coin cell format. The minimum stoichiometry $y_{min}^{Pouch,NMC}$ is determined considering the first delithiation step leading to a minimum stoichiometry of 0.259 equals to the value obtain in the coin cell format.

For the negative electrode, the amount of used capacity in the pouch format is only 29.8 mAh, much lower than the 53 mAh available capacity. It corresponds to a reversible capacity $Q_{rev}^{Pouch,Gr}$equals to 205 mAh/g. By Assuming that the minimum stoichiometry for graphite in the pouch cell format is the same than in the coin cell format ($y_{min}^{Pouch,Gr} = 0.045$), the value of the full lithiation in the case of pouch system is expressed as:

$$y_{max}^{Pouch,Gr} = y_{min}^{Pouch,Gr} + \frac{Q_{rev}^{Pouch,Gr}}{Q_{th}^{Gr}} \quad (5)$$

It leads to a value of 0.598, lower than the one in CC format.

Finally, the stoichiometry of the active materials in each electrode can be related to every SOC of the cell (Fig. 3b) using the following relations:

$$y_{NMC} = -\left(y_{max}^{Pouch,NMC} - y_{min}^{Pouch,NMC}\right) SOC + y_{max}^{Pouch,NMC} \quad (6)$$

$$y_{Gr} = \left(y_{max}^{Pouch,Gr} - y_{min}^{Pouch,Gr}\right) SOC + y_{min}^{Pouch,Gr} \quad (7)$$

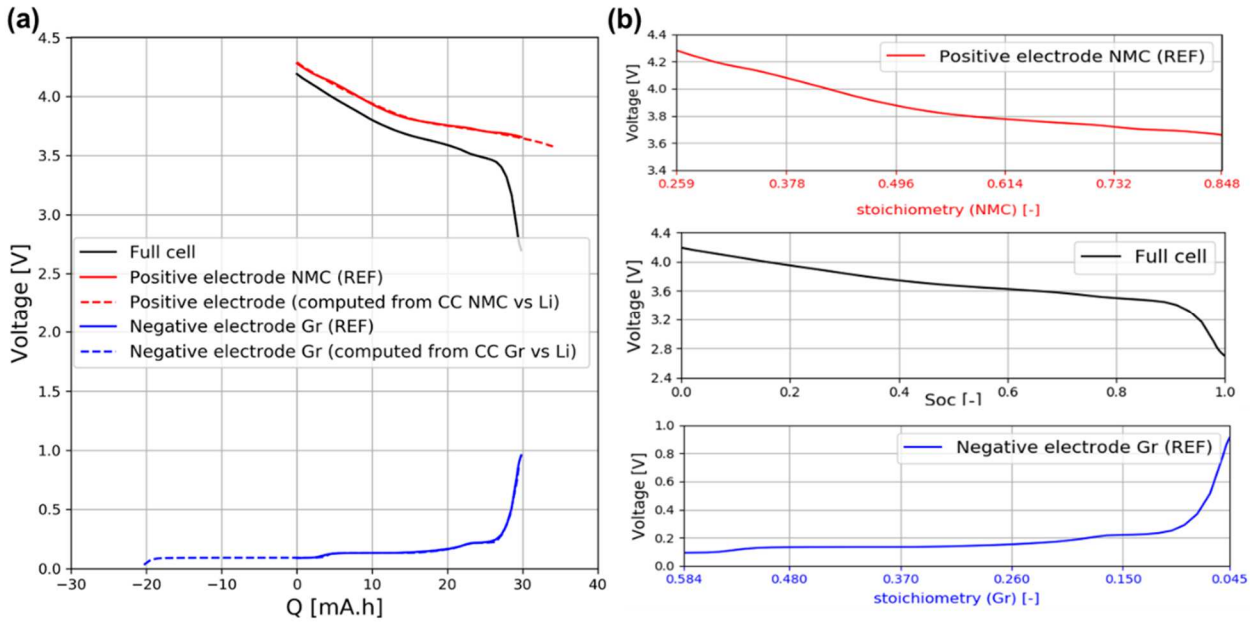

Fig. 3: (a) Pouch cell OCP curves as function of the cell capacity with the positive and the negative electrodes potentials measured with the reference electrode (labeled REF) compared to the positive and negative electrodes potentials computed from the coin cells (CC) measurements , (b) OCP curves of the full cell and positive and negative electrodes as function of the cell SOC and active materials stoichiometry

3.2 Diffusion coefficient in active materials

The chemical diffusion coefficient is determined from the transient voltage responses during the pulses at constant current of the GITT experiment in coin cell design. To that end we use Eq. (8) which has been developed in [34], [17], [1] from the analytical solution of diffusion processes in a planar geometry. For this geometry, the solution of the diffusion problem can be expressed as an infinite series of error functions. For the spherical geometry, the analytical solution is developed in the literature only in Fourier series [36], which do not converge rapidly for short times. Nevertheless, Smith et al. [37] have shown, by using an empirical development of the Fourier series at short time, that the development proposed to estimate the diffusion coefficient for the planar geometry is also valid for the spherical one.

$$D_s = \frac{4}{\pi}\left(\frac{V_M I_0}{S_{AM} F z_i}\right)^2 \left[\frac{dE_q}{dy} \Big/ \frac{dE}{d\sqrt{t}}\right]^2 \qquad t \ll {r_s}^2 \Big/ D_s \tag{8}$$

I_0 is the applied constant current during the pulse, V_M the active material molar volume, z_i the number of electron exchanged during the (de)-insertion reaction, and equals to 1, F the Faraday constant and S_{AM} the exchange area in CC design between the electrolyte and the

active material particles. $\frac{dE_q}{dy}$ is the slope of the equilibrium potential vs. the stoichiometry y. Equation 8 assumes a diffusion Fick's law, a small diffusion length compared to the dimension of the particle as well as a negligible volume changes.

$\frac{dE}{d\sqrt{t}}$ can be obtained from the plot of the transient voltage versus the square root of time during the constant current pulse. To choose the right time domain, the linearity of the transient voltage versus the square root of time has been checked for each pulse. For the positive electrode, Fig. 4a shows the typical transient voltage response obtained during one of the pulse at C/10 as function of time for the first 250s of the pulse. At beginning of the pulse, the voltage varies linearly with the square root of time, as illustrated Fig. 4b. A similar behavior is obtained for the negative electrode in the single-phase regions, as illustrated Fig. 5. This confirms that the GITT-obtained diffusion values for these stoichiometries are accurate and that the slope from the curve fit can be used in Eq.8 [38] [39] [34]. The physical parameters used in the data treatment are summarized Table 1. The values obtained for the diffusion coefficients for both active materials are displayed Fig. 6 as function of the stoichiometry of each electrode.

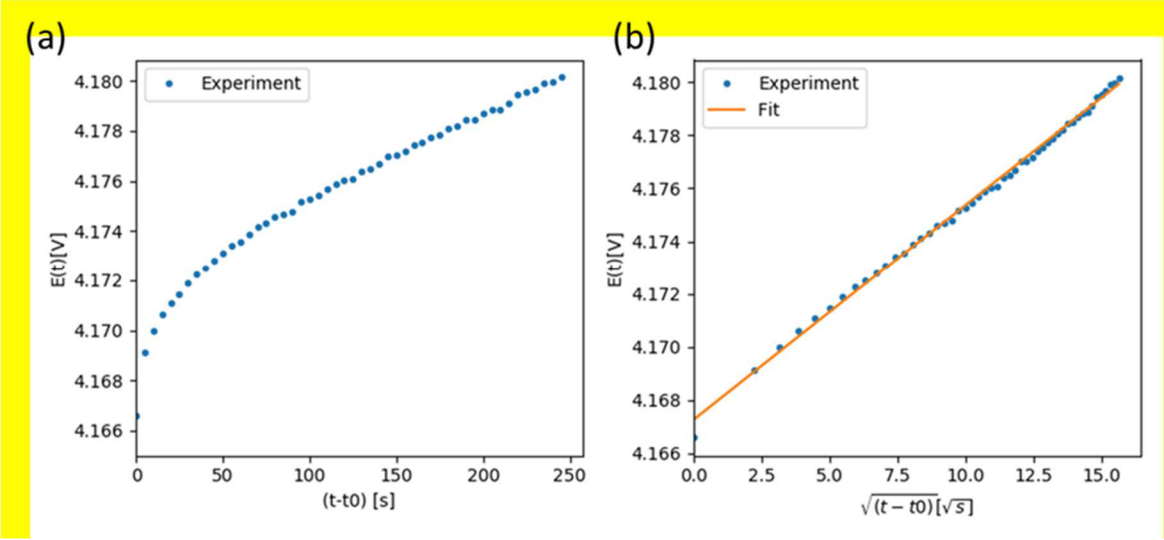

Fig. 4 : $Ni_{0.6}Mn_{0.2}Co_{0.2}O_2$ vs. Li GITT experiment (a) Cell voltage as a function of time during a charging current pulse (b) Cell voltage vs square root time for the same charging current pulse with the corresponding linear fit

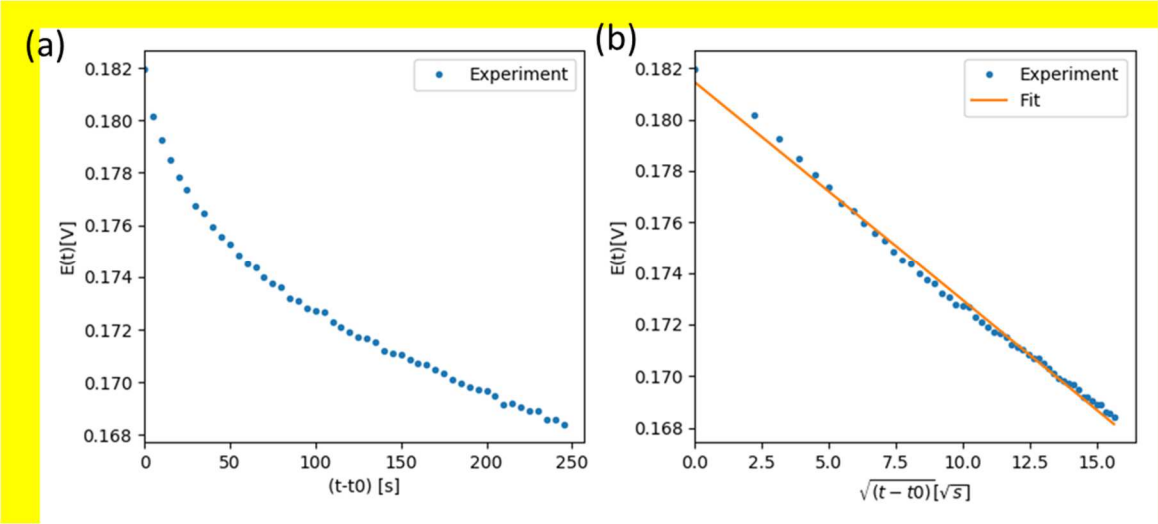

Fig. 5: Graphite vs. Li GITT experiment (a) Cell voltage as a function of time during a discharging current pulse (b) Cell voltage vs square root time for the same discharging current pulse with the corresponding linear fit

Table 1: Parameters used to extract the graphite and $Ni_{0.6}Mn_{0.2}Co_{0.2}O_2$ diffusion coefficients (CC design) and exchange current densities (Pouch design)

Parameter	**Value**			
	Graphite	$Ni_{0.6}Mn_{0.2}Co_{0.2}O_2$	Source	Error
$\boldsymbol{I_0(A)}$ **during pulse**	5.5e-4	4.6e-4	calculated	-
$\boldsymbol{V_M(m^3.mol^{-1})}$	5.31e-6	12.35e-6	calculated	-
$\boldsymbol{r_{50}(m)}$	7.88e-6	6.6e-6	Measured	± 1.8µm
$\boldsymbol{L\ (m)}$	72e-6	66e-6	Measured	± 1µm
$\boldsymbol{S_g(m^2)}$ **in CC design**	1.5e-4	1.5e-4	calculated	-
$\boldsymbol{S_{AM}(m^2)}$ **in CC design**	2.68e-4	3.31e-4	calculated	-
$\boldsymbol{S_g(m^2)}$ **in pouch design**	12.25e-4	10.24e-4	calculated	-
$\boldsymbol{S_{AM}(m^2)}$ **in pouch design**	22.28e-4	22.03e-4	calculated	-

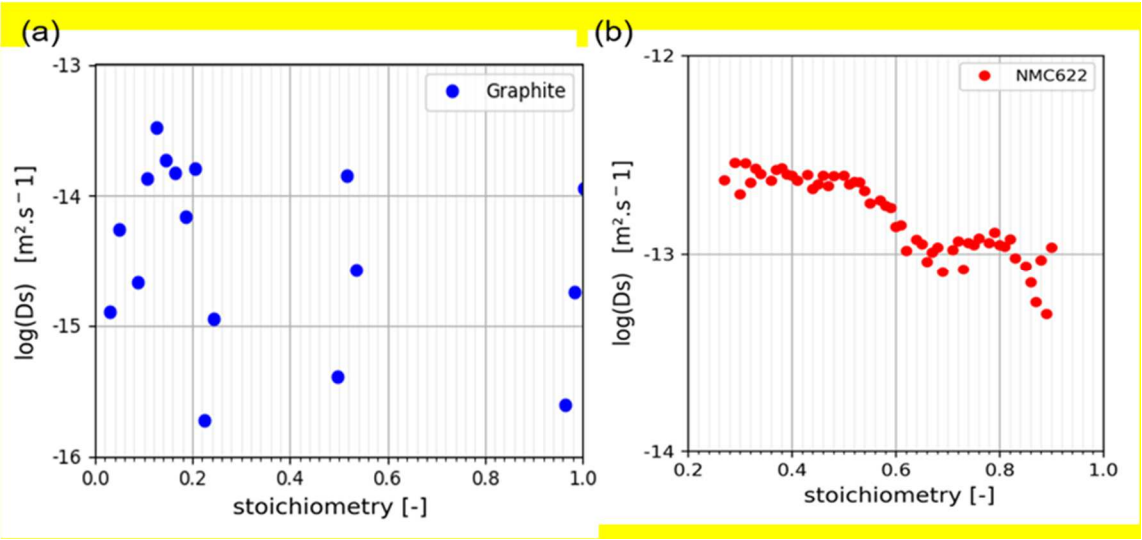

Fig. 6: Base 10 logarithm of the diffusion coefficient vs stoichiometry: (a) graphite, (b) $Ni_{0.6}Mn_{0.2}Co_{0.2}O_2$

The diffusion coefficient measured with this technique is a function of the derivative of the potential with respect to the stoichiometry, $\frac{dE_q}{dy}$. The interpretation of the measurement relies on Fick's law, which accounts for diffusion in one phase. For the graphite electrode, two phases can co-exist, which leads to a plateau in the equilibrium potential of graphite (See Fig. 2a) where $\frac{dE_q}{dy}$ is almost zero. As the present technique is not adequate to extract diffusion coefficients in these two-phase regions, we choose to not display the points obtained on the plateaus on Fig. 6a, but only those corresponding to the transition regions. For the three regions (stoichiometries below 0.25, stoichiometries around 0.5 and stoichiometries above 0.95), the values are between 1E-15 and 1E-14 $m^2\ s^{-1}$ without a clear tendency regarding the dependence on the stoichiometry. The order of magnitude and the overall tendencies are nevertheless coherent with results reported in the literature for graphite, whose values are in the range [1E-15 – 1E-13] $m^2\ s^{-1}$ in [6], or [3E-15 and 1.E-12] in [40].

For $Ni_{0.6}Mn_{0.2}Co_{0.2}O_2$, a regular monotone decrease of the diffusion coefficient can be observed in Fig. 6b. D_s values are varying between 1E-13 and 5E-13$m^2\ s^{-1}$ over the entire stoichiometry compared to the values proposed in the literature [1E-16 – 1E-11] $m^2\ s^{-1}$ [41]. An almost constant value around 5E-13$m^2\ s^{-1}$ is obtained for stoichiometry below 0.49, while a slight decrease is observed until stoichiometry of 0.64, with a subsequent stabilization at a value around 1E-13 $m^2\ s^{-1}$ for the highest stoichiometry values. These three domains

might be related to the structure changes of the $Ni_{0.6}Mn_{0.2}Co_{0.2}O_2$ active material [42] [43]. This material undergoes phase transition from pristine hexagonal H1 phase to subsequent hexagonal H2 and H3 phases. Although *ex-situ* and operando XRD measurements have been reported recently [43], the cognition of the structural difference between these phases and their precise stoichiometry range remains not fully understood. In our measurements, the domain of stoichiometry above 0.64 could related to the region where H1 and H2 structures coexist and the second domain [0.49 – 0.64] to a region where only the H2 structure is existing, while the last domain [0.26 – 0.49] to a region where a transition between H2 and H3 structures manifests.

3.3 Exchange current density

The aim of this section is to determine the exchange current densities of the two active materials from the EIS measurements carried out in the pouch cell design with two reference electrodes. Fig. 7 displays the Nyquist plots of the EIS obtained for the negative electrode (a), full cell (b) and positive electrode (c) at the different states of charge of the cell. Whatever the system, the Nyquist plots consist of an out-of-shaped semicircle alike in appearance of a half ellipse in high and intermediate frequency ranges and a straight line inclined at a constant angle to the real axis in the lower frequency range. The first capacitive arc is related for a part to the charge transfer phenomenon from where the i_0 values for the two electrodes can be fitted. The flattened shape can be observed in the case of porous electrodes with limited electronic or ionic conductivities [44]. The straight-line in the low frequency limit is due to diffusion phenomena which can be described with a Warburg contribution. For a better identification of the different physical domain in the spectra, a presentation of the imaginary part of the impedance vs. frequency is shown in Fig. 6 for the two electrodes. This figure allows to determine the characteristic frequency of the charge transfer (f_{max}), which corresponds to the highest point of the semi-circle in the Nyquist plots. The second identified characteristic frequency is the one corresponding to the minimum value of the imaginary part of the impedance while going to low frequency ($f_{\min}$). This frequency represents the limit between the interfacial phenomena (charge transfer resistance) and the bulk phenomena (lithium transports in particles and electrolyte).

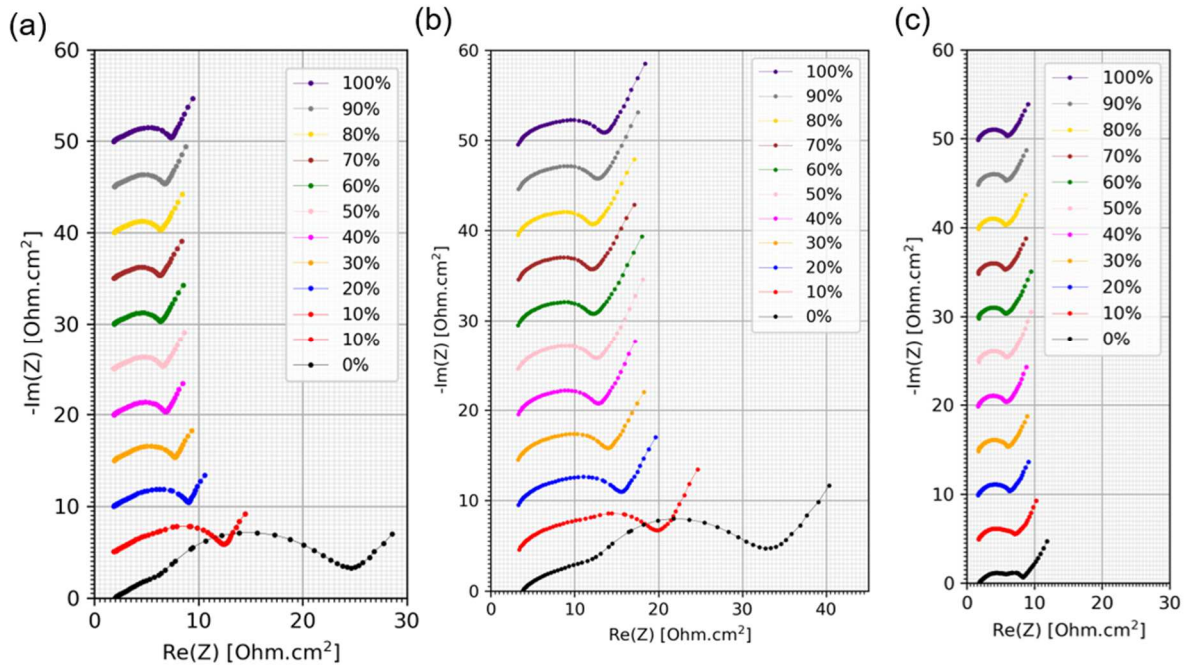

Fig. 7: EIS spectra of the 4-electrode pouch cell in Nyquist plot at different SOC: (a) negative electrode (graphite), (b) full cell and (c) positive electrode ($Ni_{0.6}Mn_{0.2}Co_{0.2}O_2$), with a shift of 5 ohm.cm² between two successive SOC

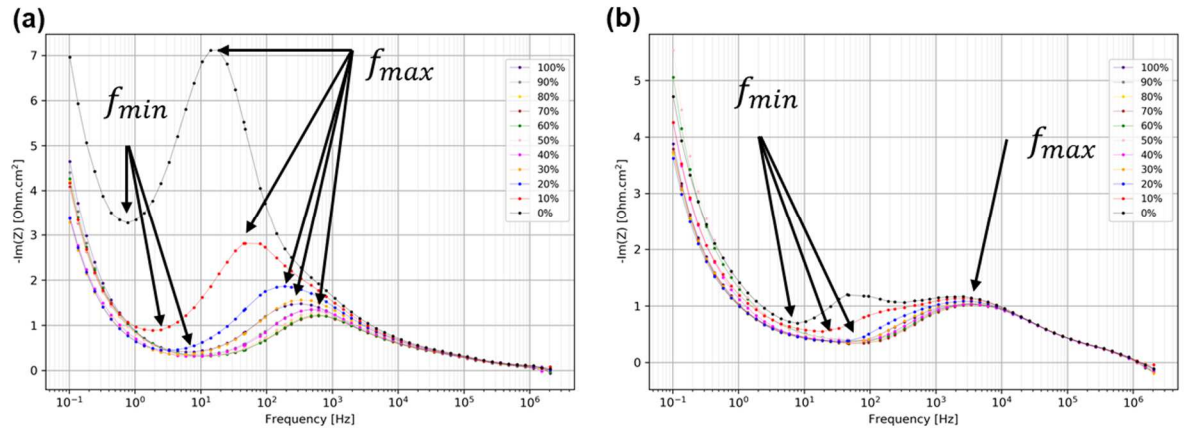

Fig. 8: EIS spectra of the 4-electrode pouch cell at different SOC represented with -Im(Z) vs frequency: (a) negative electrode (graphite), (b) positive electrode ($Ni_{0.6}Mn_{0.2}Co_{0.2}O_2$)

For the graphite, the physical phenomenon representing the AM/electrolyte interface in the EIS diagrams is in the intermediate to high frequency domain. As shown in fig. 5a, the magnitude of the flattened semi-circle corresponding to the charge transfer resistance decreases when the SOC of the cell increases. For a SOC higher than 20%, f_{max} and $f_{\min}$are rather constant as can be seen Fig. 6a, which reflects a stable interface electrochemistry. However, for a SOC between 20% and 0%, $f_{\min}$ decreases a lot, going from values around

260 Hz for SOC of 100% to values around 19 Hz at 0% SOC (Fig. 6a) suggesting a slower charge transfer for a lower SOC [30].

For $Ni_{0.6}Mn_{0.2}Co_{0.2}O_2$ (Fig. 5.c), EIS spectra are quite similar to the negative ones, but with an overall lower magnitude. For a SOC higher than 30%, all the diagrams have the same flattened semicircles shape with a constant width. Conversely, two flat semicircles shape can be distinguished with a width increase when the SOC decreases from 20% to 0%. As presented in fig. 6.b, f_{max} and $f_{\min}$are the same over a large SOC range of [30%- 100%]. However, they increase from 20% to 0%. The same behavior, for a SOC below 30%, was reported for other materials similar to $Ni_{0.6}Mn_{0.2}Co_{0.2}O_2$, like $LiMn_2O_4$ [29] and $LiNi_{0.8}Co_{0.15}Al_{0.05}O_2$ [45]. In these works, the high frequency arc was associated to the Li^+ migration through the oxide layer film and the second one between the higher and middle frequency to the charge transfer resistance.

EIS measurements are fitted to extract the exchange current densities of both graphite and $Ni_{0.6}Mn_{0.2}Co_{0.2}O_2$ active materials. To reach this goal, the capacitive arc of the different spectra should be analyzed quantitatively by using EEC model. As mentioned before, simple R-C element model is usually implemented by assuming a semi-circle shape of the capacitive arc, which is not observed in the present case (see fig. 5). In fact, porous electrodes have a potential gradient along the electrode layer thickness. Thus, TLM model is employed in order to analyze EIS spectra, by considering electronic and ionic paths through the solid phase and the electrolyte in the pores respectively [29], [16]. For porous LIB electrodes, the electronic conductivity is much higher than the ionic one. Therefore, electronic resistance can be neglected, and the TLM [46] impedance is reduced to:

$$Z_{TLM} = \lambda\chi \coth\left(\frac{L}{\lambda}\right) \tag{9}$$

The resistance per unit length χ related to the ionic path is defined as:

$$\chi = \frac{1}{\sigma_e} \tag{10}$$

The ionic conductivity σ_e is equal to 1 mS/cm at 25°C for the studied electrolyte. This model takes into account the charge transfer at the interface between active materials and the

electrolyte, via the introduction of λ, the characteristic alternating current penetration depth in the electrode defined by:

$$\lambda = \sqrt{\frac{Z_{int}\, L}{\chi}} \tag{11}$$

The values of the electrode thickness L are provided in table 1 for the positive and negative electrodes respectively. The area-specific impedance Z_{int} of the electrochemical reaction taking place at the interface, is modeled as a simple parallel combination between the charge transfer R_{ct} and a constant phase element (CPE) [15]:

$$Z_{int} = \frac{R_{ct}}{1 + (i\omega R_{ct} C)^n} \tag{12}$$

with

$$R_{ct} = \frac{RTS_g}{Fi_0 S_{AM}} \tag{13}$$

S_g is the geometric area in the pouch design, S_{AM} is the AM exchange area in the pouch design, R is gas constant, T is the temperature, F is the Faraday's constant and i_0 is the exchange current density. A procedure was adopted to fit, with this TLM model, the capacitive arc of the experimental EIS spectra (Fig. 5a-c) corresponding to the charge transfer phenomenon for each value of the SOC in the frequency range between f_{min} and 200kHz. The used parameters are presented in Table 1. This method allows us to extract the values of i_0 for each stoichiometry value for both PE and NE, *via* Eq. (13).

The obtained results are presented Fig. 9a. as function of the active material stoichiometries. For the graphite, the experimental curve of exchange current density is asymmetric; with values ranging between 0.8 and 8.4 A/m², which is consistent with the values reported in the literature [47], [48] that show large variation: between 0.5 and 35 A/m². For the $Ni_{0.6}Mn_{0.2}Co_{0.2}O_2$, the experimental curve has a more symmetric shape compared to the graphite. The exchange current densities obtained as function of the stoichiometry are in the

range of 2.3-4.8 A/m², in agreement with the values proposed in the literature that are in the range [0.1-6] A/m² [6], [49].

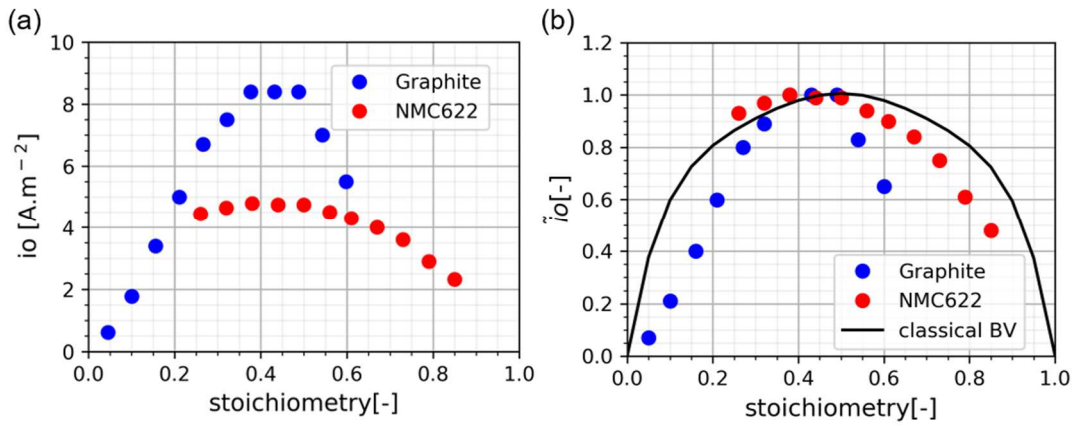

Fig. 9: Exchange current density vs. Stoichiometry: (a) for $Ni_{0.6}Mn_{0.2}Co_{0.2}O_2$ and graphite, (b) dimensionless version for comparison with the Butler-Volmer relation using $\alpha = 0.5$ (classical BV) *[50]*

4. Theoretical discussion

In earlier studies on lithium iron phosphate ($LiFePO_4$) [51], [23], it has been reported that the variation of the exchange current density with the stoichiometry is different from the Butler-Volmer approach classically used in porous electrode theory [20]. This discrepancy is also observed in the present study for the positive and the negative electrodes as shown in Fig. 7.b, where the dimensionless measured exchange current densities are compared to the Butler-Volmer results using $\alpha = 0.5$. Furthermore, in these works, the interdependence between the different active material properties is highlighted. In this study, we will follow a similar approach to analyze the link between the different material properties focusing on the molecular interactions (repulsive or attractive forces) and their impact on the active material properties. Indeed, these interactions are usually traduced in solid activity coefficients, which are used to express either the equilibrium potential or the solid diffusion. In the following, a methodology is applied to extract the values of the non-ideal interactions' energies for the positive active material, *i.e.* $Ni_{0.6}Mn_{0.2}Co_{0.2}O_2$, and we present an analytic model for the three active material properties, namely the equilibrium potential, the diffusion coefficient, as well as the exchange current density.

4.1 Theoretical framework

To express the equilibrium potential (E_q) of a Li-ion intercalation electrode, experimental profiles are usually fitted with an empirical expression due to the lack of understanding of the solid-state redox reactions. In this study, a modified Nernst equation is used [52], which is function of liquid and solid activity coefficients respectively (γ_l, γ_s) and of the insertion rate $\theta = C_s/C_s^{max}$.

$$E_q = \frac{RT}{F} ln\left(\frac{\gamma_l}{\gamma_s \theta}\right) + E_0 \tag{14}$$

where E_0 includes the reference potential, as well as all terms which are not stoichiometry dependent. Since for the studied materials, the insertion rate and the stoichiometry are equals, we will only refer to the stoichiometry in the following. From a thermodynamic point of view, the solid coefficient activity, γ_s, accounts for lithium ion interactions with the vacant sites and the intra-molecular interactions between the lithium ions and maybe to other non-ideal interactions with the host structure. Considering a regular solution model [52], [53], the solid coefficient activity can be expressed as follows:

$$\gamma_s = \frac{1}{1-y} \exp\left(\frac{1}{RT}(e_s + e_1 y + e_2 y^2)\right) \tag{15}$$

The term in the exponential accounts for the non-ideal interactions. A quadratic expression was chosen for the intercalation energy factor to account for both lithium-vacant site and lithium-lithium interactions. e_s is the interaction energy between lithium and the solid host materials, which is an attractive interaction and should be negative [54]. Note that e_1 and e_2 are the coefficients of a polynomial function of the interaction energy representing the lithium-lithium interactions in the same layer and between the neighboring layers. To simplify the up-coming demonstrations, the non-dimensional form of these energies is introduced ($\varepsilon_i = e_i/RT$). By using the solid activity coefficient definition (Eq. (15)), the equilibrium potential can be expressed as follows:

$$E_q = \frac{RT}{F}\left[\ln(\frac{1-y}{y}) - (\varepsilon_s + \varepsilon_1 y + \varepsilon_2 y^2)\right] + E_0' \tag{16}$$

Where E_0' is a constant. The driven force for the diffusion flux can be defined using either the chemical potential gradient or the concentration gradient. Considering these two latter definitions, the chemical solid diffusion coefficient can be obtained as shown in [17] as:

$$\frac{D_s}{D_0} = \frac{\partial \ln(\gamma_s y)}{\partial \ln(y)} \tag{17}$$

D_0 is the tracer diffusivity deduced from the chemical potential gradient used to express the flow. By using the expression of the equilibrium potential E_q (Eq. (16)), it is possible to explicit the link between these two parameters:

$$\frac{D_s}{D_0} = -y\frac{F}{RT}\frac{dE_q}{dy} \tag{18}$$

and the dependence of the diffusion coefficient on the stoichiometry, can be made explicit:

$$\frac{D_s}{D_0} = y\left[\frac{1}{y} + \frac{1}{(1-y)} + \varepsilon_1 + 2\varepsilon_2 y\right] \tag{19}$$

Similarly, the exchange current density (i_0) for intercalation electrodes can be expressed as function of the solid coefficient activity (Eq. (15)). This expression is derived from the general expression of the Butler-Volmer equation for concentrated solution proposed by Bazant [52]:

$$i_0 = \frac{i_{00}}{\gamma_a}(\gamma_s y)^{\alpha} \tag{20}$$

α is the symmetry factor of the charge transfer, i_{00} is a kinetic constant which is stoichiometry independent and γ_a is the activity coefficient of the transition state. Considering a fixed number n, of excluded sites, during the intercalation process, the activity coefficient can be modeled as:

$$\gamma_a = \frac{1}{(1-y)^n}\exp(\varepsilon_a) \tag{21}$$

ε_a is the intercalation energy factor of the transition state, which does not depend on the stoichiometry. These developments lead to the following expression of i_0 as function of the intercalation energies (e_s, e_1, e_2) or to simplify ($\varepsilon_s, \varepsilon_1, \varepsilon_2$):

$$i_0 = {i_{00}}' y^{\alpha}(1-y)^{(n-\alpha)} \exp\left(\alpha\left(\varepsilon_s + \varepsilon_1 y + \varepsilon_2 y^2\right)\right) \quad (22)$$

The non-stoichiometry dependent terms have been gathered in the pre-factor ${i_{00}}'$.

4.2 Theoretical results

$\varepsilon_s, \varepsilon_1$ and ε_2 are determined from the experimental results. The simulated E_q (Eq. (16)), D_s (Eq. (8)) and i_0 (Eq. (22)) are compared to the experimental measurements. We have limited our study to the positive electrode active material, *i.e.* the $Ni_{0.6}Mn_{0.2}Co_{0.2}O_2$, as the multi-phase behavior of graphite is more complex to apprehend without resorting to multi-phasic theories.

The interactions energy factors have been determined from the equilibrium potential of the $Ni_{0.6}Mn_{0.2}Co_{0.2}O_2$ material by using Eq. (16). To obtain a good fit over the whole stoichiometry range, we have distinguished three stoichiometry zones in which each intercalation factor has a constant value that changes from one zone to another. These three different zones could account for the host material structure modification upon intercalation as reported in [42], [43]. The obtained values for the coefficient of the second order polynomial are given table 2, by using an empirical value for ${E_0}'$ equals to 3.798 V.

Table 2: Fitted values of interaction energies

Stoichiometry zone	$\boldsymbol{\varepsilon_s}$ $[-]$	$\boldsymbol{e_s}$ $[\boldsymbol{eV}]$	$\boldsymbol{\varepsilon_1}[-]$	$\boldsymbol{e_1}[\boldsymbol{eV}]$	$\boldsymbol{\varepsilon_2}$ $[-]$	$\boldsymbol{e_2}[\boldsymbol{eV}]$
zone 1(0,26 <y < 0,49)	-38.09	-0.98	91.13	2.34	-38.94	-1
zone 2 (0,49 <y< 0,64)	-59.17	-1.52	177.89	4.57	-129.81	-3.34
zone 3 (0,64 <y< 0,9)	-4.95	-0.13	3.89	0.1	8.76	0.23

The result of the fit is displayed Fig. 10a, which shows an excellent agreement between the experimental result and the analytic expression for the equilibrium potential, the average

deviation being below 2 mV. Therefore, Eq. (16) can be implemented to express the equilibrium potential of the $Ni_{0.6}Mn_{0.2}Co_{0.2}O_2$ instead of using empirical data. To get a global view of the interactions inside the solid active material, the sum of the interaction energies, $-(\varepsilon_s + \varepsilon_1 y + \varepsilon_2 y^2)$ is displayed Fig. 10b. Even though we have used a second order polynomial, the dependence remains rather linear in two regions, at low and high stoichiometries. Such linear dependency was also reported for Li_xTiS_2 [55] with an interaction energy modeled as A.y with A=220meV.

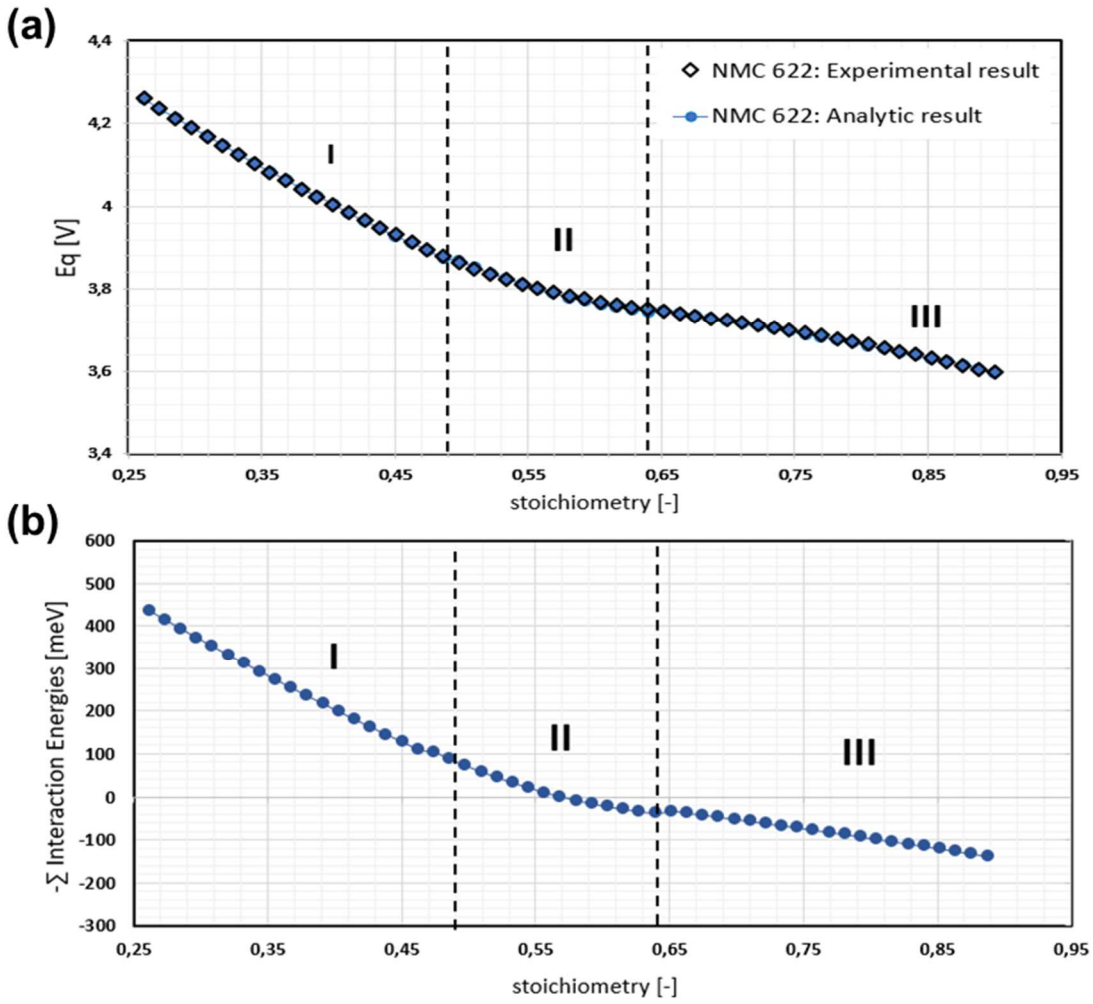

Fig. 10: (a) $Ni_{0.6}Mn_{0.2}Co_{0.2}O_2$ equilibrium potential. Validation of the analytic expression by comparison to the experimental results. (b) Sum of the interaction energies for the $Ni_{0.6}Mn_{0.2}Co_{0.2}O_2$ active material as function of the stoichiometry

For the diffusion coefficient D_s, Eq. (8) is implemented using the values of the intercalation energies factors determined previously (table 2). A good agreement with the experimental data throughout the entire stoichiometry (Fig. 11a) is achieved when D_0 is defined as a function of the square root of the stoichiometry:

$$D_0 = \frac{A}{\sqrt{y}} \tag{23}$$

considering a parameter A equal to $6.25\ 10^{-15} m^2\ s^{-1}$.

More precisely, two different zones can be distinguished. In the first one, for a stoichiometry lower than 0.64, the analytic model matches very well the experimental data. Conversely, for higher stoichiometry, the analytical equation for D_s does not fit well with experimental data. This difference for high stoichiometry between [0.64-0.9] may be due to non-ideal behavior of the active material and other interactions than the intra-molecular interactions. To get a better result (Fig. 11.b), D_0 was modified for this part of stoichiometry and expressed as:

$$D_0 = \frac{A'}{\sqrt{y}}(1-y)^{0.3} \tag{24}$$

Where the parameter A' is equal to $8.99\ \ 10^{-15} m^2.s^{-1}$.

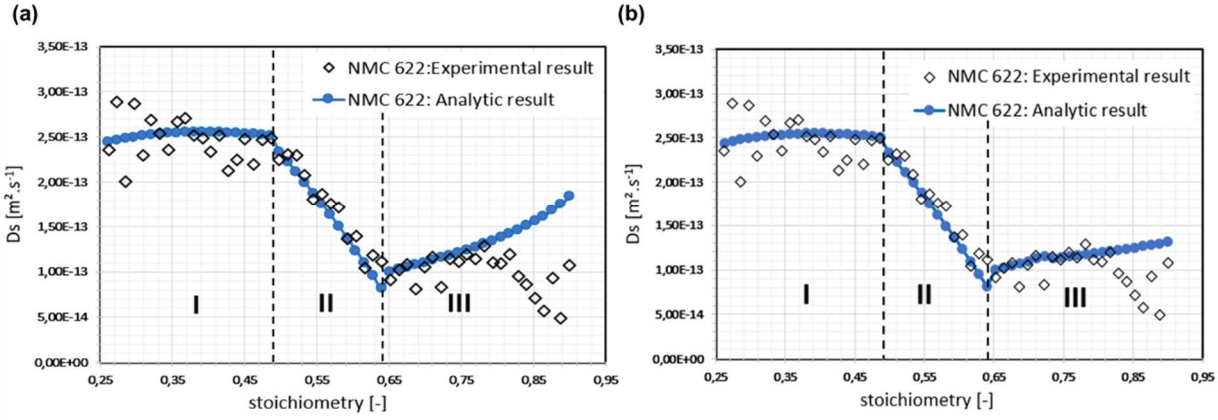

Fig. 11: Validation of the model equation of the $Ni_{0.6}Mn_{0.2}Co_{0.2}O_2$ D_s

Regarding the exchange current density, Eq. (22) has been implemented using the intercalation energies factors presented in table 2. The analytic curve was fitted with n=0.75, $\alpha = 0.023$ and $i'_{00} = 8.5\ A.m^{-2}$ with an average deviation of 0.073 $A.m^{-2}$. A visual inspection of the plots (Fig. 12) reveals a very good agreement for all the stoichiometry range. Therefore, Eq. (22) leads to a better agreement than the one obtained with the classical Butler-Volmer expression (Fig. 9.b), for which an average deviation of 0.39 $A.m^{-2}$ from the experimental result was obtained. Thus, taking into consideration the impact of the non-ideal

interactions reduces three times the average deviation. However, the fitted value for the symmetry factor α is very small, in order to limit the impact of the interaction energies on the exchange current density. Since the reported value for α is much lower than expected, compared to the one proposed with classical BV equals to 0.5, we report for comparison another solution based on the modified Butler-Volmer relation without taking into account the non-ideal interaction energies. In this case Eq. (22) reduces to:

$$i_0 = i_{00}{}' y^{\alpha}(1-y)^{(n-\alpha)} \tag{25}$$

The best fit is obtained considering that the number of excluded sites, n, is equal to 2, and α is equal to 0.9. The corresponding result is displayed Fig. 12. This analytic model is also very close from the experimental data, an average deviation of 0.129 $A.m^{-2}$ being achieved.

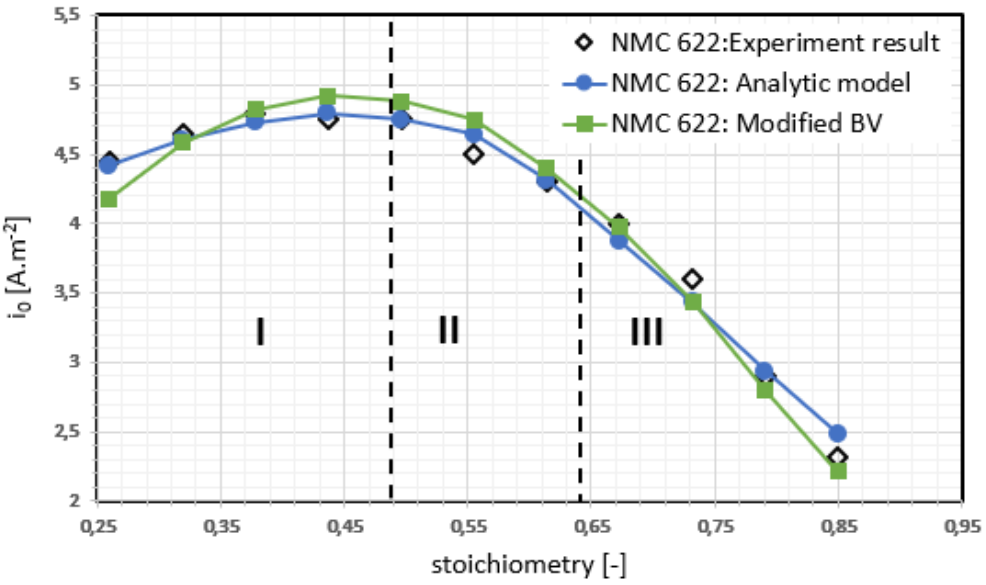

Fig. 12: Validation of the model equation of the $Ni_{0.6}Mn_{0.2}Co_{0.2}O_2$ i_0

In this part, an effort has been made to explicit the link between the three active material properties (the equilibrium potential, E_q, the diffusion coefficient, D_s and the exchange current density, i_0) using thermodynamic relations available in the literature. Based on these relations, we find some unexpected results. For example, for the solid diffusion coefficient, generally, it is related to the derivative of the equilibrium potential via the stoichiometry and not the square root of the stoichiometry, as reported here. Likewise, the analytic expression of the exchange current density developed in this work leads to assign a very small value to the symmetry factor to limit the impact of the interaction energies and to be able to match the experimental results. This result is rather unexpected and leads to think about another

significant interaction energy which should be taken into account. This supplementary term might arise from a concentration gradient of the lithium at the active particle surface [52] due to very localized structural modifications. Indeed, spinel and rocksalt phases often form as thin layered on the surface of layered intercalation compounds, which might modify very locally the interaction energies [56]. This type of development, taking into consideration the heterogeneities inside the active material, goes however beyond the scope of this work, but seems crucial if we wish to keep a thermodynamic consistency to describe the different active material physical parameters.

5. Conclusion

In this paper, we have presented a consistent route to measure and extract the values of three of the most significant active material physical properties, namely the equilibrium potential, the diffusion coefficient and the exchange current density, as function of the stoichiometry of the active materials. The *de Levie*'s model has been used to retrieve the exchange current densities of the two porous electrodes from EIS spectra measured using $LiFePO_4$ as a reference electrode. The link between the three measured properties has been then further discussed using a general thermodynamic approach. Focusing on the $Ni_{0.6}Mn_{0.2}Co_{0.2}O_2$ positive material, the interaction energies have been determined and analytical expressions for the diffusion coefficient and exchange current densities have been suggested. The thermodynamic relations available in the literature are not directly transposable to the $Ni_{0.6}Mn_{0.2}Co_{0.2}O_2$ material, suggesting the necessity to account for supplementary terms. Nevertheless, the proposed stoichiometry dependent laws determined with the same stoichiometry definition go already beyond most reported values for the $Ni_{0.6}Mn_{0.2}Co_{0.2}O_2$ and can be used to increase the predictability of multi-physics lithium-ion battery models.

Acknowledgements

This work has received funding from the French National Association of Research and Technology (CIFRE 2017/0705). We are grateful to Yvan Reynier for the manufacturing of the electrodes.

List of Symbols

Parameter	Symbol
Stoichiometry (-)	y
coefficient activity of the transition state (-)	γ_l
solid coefficient activity (-)	γ_s
Symmetry factor of the charge transfer (-)	α
Intercalation energy factors of the lithium- vacant site (-)	ε_s
Ionic resistance ($ohm\ m$)	χ
Characteristic alternating current penetration depth in the electrode (m)	λ
Electronic conductivity ($S\ m^{-1}$)	σ_e
Polynomial coefficient of intercalation energy factors of the lithium- vacant site and lithium-lithium (-)	ε_1
Polynomial coefficient of intercalation energy factors of the lithium- vacant site and lithium-lithium (-)	ε_2
Capacitance (F m^{-2})	C
Diffusion coefficient of Lithium in the active material ($m^2\ s^{-1}$)	D_s
Polynomial coefficient of intercalation energy of the lithium- vacant site and lithium-lithium (meV)	e_1
Polynomial coefficient of intercalation energy of the lithium- vacant site and lithium-lithium (meV)	e_2
Intercalation energy of the lithium- vacant site (meV)	e_s
Equilibrium potential (V)	E_q
Faraday's constant (96487$C\ mol^{-1}$)	F
Applied constant current during the pulse (A)	I_0
Exchange current density ($A\ m^{-2}$)	i_0
Electrode's thickness (m)	L
Capacity (mAh)	Q
Gas constant (8.314 $J\ mol^{-1}K^{-1}$)	R
Charge transfer resistance ($ohm\ m^2$)	R_{ct}
Exchange area (m^2)	S_{AM}
Geometric area (m^2)	S_g
state of charge of the cell (-)	Soc
Transmission line model ($ohm\ m^2$)	TLM
Temperature (K)	T
Molar volume($m^3\ mol^{-1}$)	V_M
Area-specific impedance of the electrochemical reaction taking place at the interface ($ohm\ m^2$)	Z_{int}
TLM impedance ($ohm\ m^2$)	Z_{TLM}
Number of electron exchanged during the (de)-insertion reaction (-)	z_i

References

[1] D. Gruet, B. Delobel, D. Sicsic, I. T. Lucas and V. Vivier, "On the electrochemical impedance response of composite insertion electrodes. Toward a better understanding of porous electrodes," *Electrochimica Acta,* vol. 295, pp. 787-800, 2019.

[2] J. Randles, "Kenitics of rapid electrode reactions," *Discussions of the faraday society,* vol. 1, pp. 11-19, 1947.

[3] M. Doyle, T. F. Fuller and J. Newman, "Modeling of Galvanostatic Charge and Discharge of the Lithium/Polymer/Insertion Cell," *J. Electrochem. Soc.,* vol. 140, pp. 1526-1533, 1993.

[4] N. Dufour, M. Chandesris, S. Geniès, M. Cugnet and Y. Bultel, "Lithiation heterogeneities of graphite according to C-rate and mass-loading: A model study," *Electrochimica Acta,* vol. 272, pp. 97-107, 2018.

[5] J. Newman and W. Tiedemann, "Porous-electrode theory with battery applications," *AIChE J.,* vol. 21, pp. 25-41, 1975.

[6] M. Ecker, T. K. D. Tran, P. Dechent, S. Katz, A. Warnecke and D. U. Sauer, "Parameterization of a Physico-Chemical Model of a Lithium-Ion Battery: I. Determination of Parameters," *Journal of The Electrochemical Society,* vol. 162, pp. A1836-A1848, 2015.

[7] A. Zaban, E. Zinigrad and D. Aurbach, "Impedance Spectroscopy of Li Electrodes. A General Simple Model of the Li-Solution Interphase in Polar Aprotic Systems," *J. Phys. Chem.,* vol. 100, pp. 3089-3101, 1 1996.

[8] D. Aurbach, "Impedance Spectroscopy of Nonactive Metal Electrodes at Low Potentials in Propylene Carbonate Solutions," *J. Electrochem. Soc.,* vol. 141, p. 1808, 1994.

[9] J. Illig, J. P. Schmidt, M. Weiss, A. Weber and E. Ivers-Tiff\'ee, "Understanding the impedance spectrum of 18650 LiFePO4-cells," *Journal of Power Sources,* vol. 239, pp. 670-679, 2013.

[10] A. Martinent, B. L. Gorrec, C. Montella and R. Yazami, "Three-electrode button cell for {EIS} investigation of graphite electrode," *Journal of Power Sources,* vol. 97–98, pp. 83-86, 2001.

[11] J. G. Thevenin, "Impedance of Lithium Electrodes in a Propylene Carbonate Electrolyte," *J. Electrochem. Soc.,* vol. 134, p. 273, 1987.

[12] H. Schranzhofer, J. Bugajski, H. J. Santner, C. Korepp, K.-C. Möller, J. O. Besenhard, M. Winter and W. Sitte, "Electrochemical impedance spectroscopy study of the SEI formation on graphite and metal electrodes," *Journal of Power Sources,* vol. 153, pp. 391-395, 2006.

[13] J. Huang, H. Ge, Z. Li and J. Zhang, "An Agglomerate Model for the Impedance of Secondary Particle in Lithium-Ion Battery Electrode," *Journal of The Electrochemical Society,* vol. 161, pp. E3202-E3215, 2014.

[14] P. Arora, B. N. Popov and R. E. White, "Electrochemical Investigations of Cobalt-Doped LiMn2O4 as Cathode Material for Lithium-Ion Batteries," *Journal of The Electrochemical Society,* vol. 145,

pp. 807-815, 1998.

[15] J. Nielsen and J. Hjelm, "Impedance of SOFC electrodes: A review and a comprehensive case study on the impedance of LSM:YSZ cathodes," *Electrochimica Acta,* vol. 115, pp. 31-45, 2014.

[16] J. Illig, M. Ender, A. Weber and E. Ivers-Tiffée, "Modeling graphite anodes with serial and transmission line models," *Journal of Power Sources,* vol. 282, pp. 335-347, 2015.

[17] W. Weppner and R. A. Huggins, "Determination of the Kinetic Parameters of Mixed-Conducting Electrodes and Application to the System Li3Sb," *Journal of The Electrochemical Society,* vol. 124, pp. 1569-1578, 1977.

[18] D. W. Dees, S. Kawauchi, D. P. Abraham and J. Prakash, "Analysis of the Galvanostatic Intermittent Titration Technique (GITT) as applied to a lithium-ion porous electrode," *Journal of Power Sources,* vol. 189, pp. 263-268, 2009.

[19] E. Markevich, M. D. Levi and D. Aurbach, "Comparison between potentiostatic and galvanostatic intermittent titration techniques for determination of chemical diffusion coefficients in ion-insertion electrodes," *Journal of Electroanalytical Chemistry,* vol. 580, pp. 231-237, 2005.

[20] M. Doyle and J. Newman, "Modeling the performance of rechargeable lithium-based cells: design correlations for limiting cases," *Journal of Power Sources,* vol. 54, pp. 46-51, 1995.

[21] T. Danner, M. Singh, S. Hein, J. Kaiser, H. Hahn and A. Latz, "Thick electrodes for Li-ion batteries: A model based analysis," *Journal of Power Sources,* vol. 334, pp. 191-201, 2016.

[22] J. Sturm, S. Ludwig, J. Zwirner, C. Ramirez-Garcia, B. Heinrich, M. F. Horsche and A. Jossen, "Suitability of physicochemical models for embedded systems regarding a nickel-rich, silicon-graphite lithium-ion battery," *Journal of Power Sources,* vol. 436, p. 226834, 2019.

[23] T. R. Ferguson and M. Z. Bazant, "Nonequilibrium Thermodynamics of Porous Electrodes," *Journal of The Electrochemical Society,* vol. 159, pp. A1967-A1985, 2012.

[24] Y. Reynier, C. Vincens, C. Leys, B. Amestoy, E. Mayousse, B. Chavillon, L. Blanc, E. Gutel, W. Porcher, T. Hirose and C. Matsui, "Practical implementation of Li doped SiO in high energy density 21700 cell," *Journal of Power Sources,* vol. 450, p. 227699, 2020.

[25] M.-D. Levi, K. Gamolsky, D. Aurbach, U. Heider and R. Oesten, "Determination of the Li ion chemical diffusion coefficient for the topotactic solid-state reactions occurring via a two-phase or single-phase solid solution pathway," *Journal of Electroanalytical Chemistry,* vol. 477, pp. 32-40, 1999.

[26] M. Ender, A. Weber and I.-T. Ellen, "Analysis of Three-Electrode Setups for AC-Impedance Measurements on Lithium-Ion Cells by FEM simulations," *Journal of The Electrochemical Society,* vol. 159, pp. A128-A136, 2011.

[27] R. Tatara, P. Karayaylali, Y. Yu, Y. Zhang and L. Giordano, "The effect of electrode-electrolyte interface on the electrochemical impedance spectra for positive electrode in Li-Ion Battery," *Journal of The Electrochemical Society,,* vol. 166, pp. A5090-A5098, 2019.

[28] D. Juarez-Robles, C.-F. Chen, Y. Barsukov and P.-P. Mukherjeea, "Impedance Evolution Characteristics in Lithium-Ion Batteries," *Journal of The Electrochemical Society,* vol. 164, pp. A837-A847, 2017.

[29] I. A. J. Gordon, S. Grugeon, H. Takenouti, B. Tribollet, M. Armand, C. Davoisne, A. Débart and S. Laruelle, "Electrochemical Impedance Spectroscopy response study of a commercial graphite-based negative electrode for Li-ion batteries as function of the cell state of charge and ageing," *Electrochimica Acta,* vol. 223, pp. 63-73, 2017.

[30] I.-J. Gordon, S. Grugeon, A. Débart, G.Pascaly and S.Laruelle, "Electrode contributions to the impedance of a high-energy density Li-ion cell designed for EV applications," *Solid State Ionics,* vol. 237, pp. 50-55, 2013.

[31] M-D.Levi, V.Dargel, Y.Shilina, D. Aurbach and I.-C. Halalay, "Impedance Spectra of Energy-Storage Electrodes Obtained with Commercial Three-Electrode Cells: Some Sources of Measurement Artefacts," *Electrochimica Acta,* vol. 149, pp. 126-135, 2014.

[32] J. Costard, M. Ender, M. Weiss and E. Ivers-Tiffée, "Three-Electrode Setups for Lithium-Ion Batteries: II. Experimental Study of Different Reference Electrode Designs and Their Implications for Half-Cell Impedance Spectra," *Journal of The Electrochemical Society,* vol. 164, pp. A80-A87, 2017.

[33] R. Zeh, F. Kindermann, R. Karl, H. Gasteiger and A. Jossen, Writers, *Electrode optimization and behavior of LTO/LFP electrodes for applications in lithium ion batteries.* [Performance]. Technical University of Munich, 2019.

[34] C. J. Wen, B. A. Boukamp, R. A. Huggins and W. Weppner, "Thermodynamic and Mass Transport Properties of LiAl," *J. Electrochem. Soc,* vol. 126, no. 12, pp. 2258-2266, 1979.

[35] J. R. Dahn, "Phase diagram of LiC6," *Phys. Rev. B,* vol. 44, no. 17, pp. 9170-9177, 11 1991.

[36] H. S. CARSLAW and J. C. JAEGER, Conduction of heat in solids, Oxford: Clarendon Press, 1959.

[37] K. Smith and C. Wang, "Solid-state diffusion limitations on pulse operation of a lithium ion cell for hybrid electric vehicles," *Journal of Power Sources,* vol. 161, p. 628–639, 2006.

[38] E. Allcorn, S. O. Kim and A. Manthiram, "Lithium diffusivity in antimony-based intermetallic and FeSb–TiC composite anodes as measured by GITT," *Phys. Chem. Chem. Phys.,* vol. 17, no. 43, pp. 28837-28843, 2015.

[39] X. H. Rui, N. Ding, J. Liu, C. Li and C. H. Chen, "Analysis of the chemical diffusion coefficient of lithium ions in Li3V2(PO4)3 cathode material," *Electrochimica Acta,* vol. 55, pp. 2384-2390, 2010.

[40] S. Malifarge, B. Delobel and C. Delacourt, "Guidelines for the Analysis of Data from the Potentiostatic Intermittent Titration Technique on Battery Electrodes," *Journal of The Electrochemical Society,* vol. 164, pp. A3925-A3932, 2017.

[41] Q. Wang, C.-H. Shen, S.-Y. Shen, Y.-F. Xu, C.-G. Shi, L. Huang, J.-T. Li and S.-G. Sun, "Origin of Structural Evolution in Capacity Degradation for Overcharged NMC622 via Operando Coupled Investigation," *ACS Applied Materials & Interfaces,* vol. 9, pp. 24731-24742, 7 2017.

[42] J. Xu, E. Hu, D. Nordlund, A. Mehta, S. Ehrlich, X. Yang and W. Tong, "Understanding the Degradation Mechanism of Lithium Nickel Oxide Cathodes for Li-Ion Batteries," *ACS Applied Materials and Interfaces,* vol. 8, p. 31677−31683, 2016.

[43] S. Zheng, C. Hong, X. Guan, Y. Xiang, X. Liu, G. Xu, R. Liu, G. Zhong, F. Zheng, Y. Li, X. Zhang, Y. Ren, Z. Chen, K.Amine and Y. Yang, "Correlation between long range and local structural changes in Ni-rich layered materials during charge and discharge process," *Journal of Power Sources,* vol. 412, pp. 336-343, 2019.

[44] J. P. Meyers, M. Doyle, R. M. Darling and J. Newman, "The Impedance Response of a Porous Electrode Composed of Intercalation Particles," *Journal of The Electrochemical Society,* vol. 147, pp. 2930-2940, 2000.

[45] D. P. Abraham, D. w. Dees and S. Kawauchi, "Modeling the impedance versus voltage characteristics of LiNi(0.8)Co(0.15)Al(0.005)O(2)," *Electrochimica Acta,* vol. 53, pp. 2121-2129, 2008.

[46] R. Levie, "On the impedance of electrodes with rough interfaces," *Journal of Electroanalytical Chemistry and Interfacial Electrochemistry,* vol. 261, pp. 1-9, 1989.

[47] A. M. Colclasure and R. J. Kee, "Thermodynamically consistent modeling of elementary electrochemistry in lithium-ion batteries," *Electrochimica Acta,* vol. 55, pp. 8960-8973, 2010.

[48] E. Prada, D. Di Domenico, Y. Creff, J. Bernard, V. Sauvant-Moynot and F. Huet, "Simplified Electrochemical and Thermal Model of LiFePO4-Graphite Li-Ion Batteries for Fast Charge Applications," *Journal of The Electrochemical Society,* vol. 159, pp. A1508-A1519, 2012.

[49] P. C. Tsai, B. Wen, M. Wolfman, M. Choe, M. S. Pan, Li.Su, K.Thornton, J. Cabana and Y. Chiang, "Single-particle measurements of electrochemical kinetics in NMC and NCA cathodes for Li-ionbatteries," *Energy and Environmental Science,* vol. 11, pp. 860-871, 2018.

[50] A. J. Bard and L. R. Faulkner, Electrochemical Methods : Fundamentals and Application, 2nd ed., John Wiley and Sons, 2001.

[51] M. Z. Bazant, "Thermodynamic stability of driven open systems and control of phase separation by electro-autocatalysis," *Faraday Discussions,* vol. 199, pp. 423-463, 2017.

[52] M. Z. Bazant, "Theory of Electrochemical Kinetics based on Nonequilibrium Thermodynamics," MIT, Cambridge, USA, 2012.

[53] M. Chandesris, D. Caliste, D. Jamet and P. Pochet, "Thermodynamics and Related Kinetics of Staging in Intercalation Compounds," *The Journal of Physical Chemistry C,* vol. 123, pp. 23711-23720, 2019.

[54] P. Derosa and P. Balbuena, "A Lattice-Gas Model Study of Lithium Intercalation in Graphite," *Journal of The Electrochemical Society,* vol. 146, pp. 3630-3638, 1999.

[55] C. Déportes, M. Duclot, P. Fabry, J. Fouletier, A. Hammou, M. Kleitz, E. Siebert and J. Souquet, Electrochimie des Solides, 1994.

[56] M. Radin, S. Hy, M. Sina, C. Fang, H. Liu, J. Vinckeviciute, M. Zhang, M. S. Whittingham, Y. S. Meng and A. V. d. Ven, "Narrowing the Gap between Theoretical and Practical Capacities in Li-Ion Layered Oxide Cathode Materials," *Advanced Energy Materials,* Vols. 7, 1602888, 2017.